AGU PUBLICATIONS

JGR

Journal of Geophysical Research: Oceans

RESEARCH ARTICLE

10.1002/2014JC009938

Key Points:

- A Yakutat eddy in the Gulf of Alaska has been imaged from the seismic data
- A set of characteristics of the Yakutat eddy have been unveiled
- Triple-s (seismic, satellite, and in situ) observations of the eddy are consistent

Correspondence to:
L. T. Sun,
ltsun@scsio.ac.cn

Citation:
Tang, Q. S., S. P. S. Gulick, and L. T. Sun (2014), Seismic observations from a Yakutat eddy in the northern Gulf of Alaska, *J. Geophys. Res. Oceans*, *119*, 3535–3547, doi:10.1002/2014JC009938.

Received 27 FEB 2014
Accepted 22 MAY 2014
Accepted article online 24 MAY 2014
Published online 6 JUN 2014

Seismic observations from a Yakutat eddy in the northern Gulf of Alaska

Q. S. Tang[1], S. P. S. Gulick[2], and L. T. Sun[1]

[1]Key Laboratory of Marginal Sea Geology, South China Sea Institute of Oceanology, Chinese Academy of Sciences, Guangzhou, China, [2]Institute for Geophysics, Jackson School of Geosciences, University of Texas at Austin, Austin, Texas, USA

Abstract Recent works show that the seismic oceanography technique allows us to relate water column seismic reflections to oceanic finescale structures. In this study, finescale structures of a surface anticyclonic eddy have been unveiled by reprocessing two seismic transects acquired in the northern Gulf of Alaska using an 8 km hydrophone streamer and 6600 cu in linear airgun array in September 2008. The eddy was a typical bowl-like structure with around 55 km width and 700 m depth. It has two fringes around the eddy base and a spiral arm at the NE edge. The in situ sea surface temperature and salinity data from a shipboard thermosalinograph help to confirm our interpretations of a spiral arm shed from the warm eddy and the entrained cold water from elsewhere. Nearby the eddy and offshore the shelf-break, there is a strong frontal feature, probably the Alaska Current. The eddy likely formed offshore Yakutat shelf and transported along the offshore shelf-break by tracking the sea level anomalies. Its equivalent diameter of 65 km was measured using the along-track altimeter and the seismic constraints. It was comparable with results from the representative conventional algorithms of eddy detection. Geostrophic velocities of the eddy were estimated from the dipping seismic reflections under the assumptions of approximate isopycnals and geostrophic balance. Measured water properties including sea surface temperature, salinity, and chlorophyll revealed that eddy translation transports coastal water to the pelagic regions. Structures synthesized from CTD profiles that sampled an earlier eddy suggest that thin striae around the base might be a common feature in Gulf of Alaska eddies.

1. Introduction

The Gulf of Alaska (GoA, Figure 1a) is a highly productive region despite downwelling-favorable winds for much of the year. Mesoscale eddies play a significant role in promoting the productivity [e.g., *Okkonen et al*., 2003; *Stabeno et al*., 2004]. Gulf circulation is dominated by the cyclonic Alaskan Gyre bounded by the North Pacific Current to the south, the Alaska Current to the east, and the Alaskan Stream to the west [e.g., *Stabeno et al*., 2004]. Along the eastern boundary of the GoA, three groups of eddies (Haida, Sitka, and Yakutat eddies) have been categorized by the geographical locations of their formation sites [e.g., *Henson and Thomas*, 2008; *Ladd et al*., 2009, 2005; *Okkonen et al*., 2001; *Rovegno et al*., 2009]. These three eddy groups share many common features, including anticyclonic rotation, baroclinic structure, 80−200 km diameter, >1500 m extent below sea surface, approximately westward translation, and warm/fresh/nutrient-rich water relative to ambient basin water of the same depth [*Crawford*, 2002; *Ladd et al*., 2005, 2007; *Peterson et al*., 2005; *Rovegno et al*., 2009]. Altimeter data show that these eddies have sea surface height anomalies up to 72 cm and live up to 5 years with average translation speed of 2.5 km d^{-1} [*Crawford et al*., 2000; *Henson and Thomas*, 2008; *Ladd et al*., 2007; *Rovegno et al*., 2009].

Of the three eddy groups in the GoA, the northernmost are the Yakutat eddies which form offshore Yakutat, Alaska, where the shelf is much wider than those of the Sitka and Haida eddy formation regions. Yakutat eddies tend to stay close to the shelf as they propagate first northwestward and then turn southwestward with the Alaskan Stream. Thus they may influence cross-shelf exchange through two mechanisms: (1) by trapping coastal waters in their interior during formation with subsequent transport into the basin and (2) through interaction with the shelf-break current [*Ladd et al*., 2005, 2007; *Okkonen et al*., 2003]. Such eddy-induced shelf-slope exchange has been evidenced by the chlorophyll concentration imagery which documents cross-shelf exchange affecting the GoA ecosystems [*Ladd et al*., 2005, 2007; *Okkonen et al*., 2003].

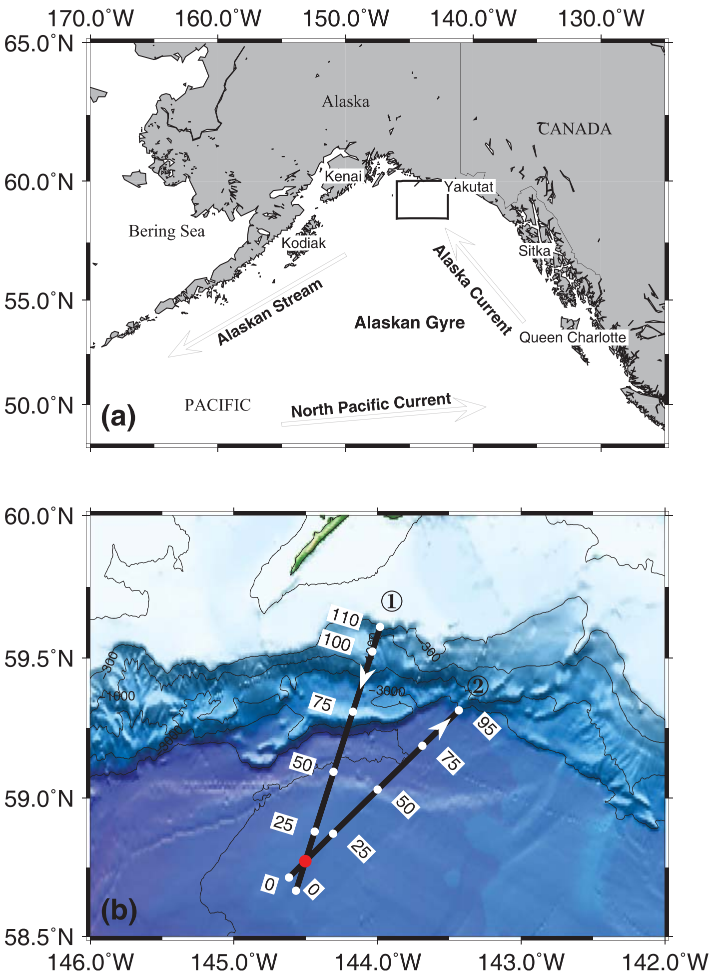

Figure 1. (a) Alaskan Gyre and geophysical features of the Gulf of Alaska. (b) Seismic transects (black lines) overlaid on the bathymetric map of the study region as outlined in (a). The white dots mark the distances (km) from the southwest. The white arrows refer to the vessel headings during seismic data acquisition. The red dot is the intersection of the seismic Line1 and Line2, whose official names are STEEP13 and STEEP07, respectively.

Although extensive conventional hydrographic observations have been carried out to study the mesoscale eddies, the ~10 km lateral resolution of these techniques hampers the ability to view detailed internal structures. A recently developed method "seismic oceanography" based on the conventional seismic reflection profiling allows us to relate water column acoustic reflections to oceanic finescale structures [e.g., *Holbrook et al.*, 2003; *Ruddick et al.*, 2009]. It has the capability of showing the mesoscale to finescale features simultaneously with a typical vertical and horizontal resolution of 10 m. Numerous oceanographic features can be outlined successfully, such as subsurface eddies [*Biescas et al.*, 2008; *Buffett et al.*, 2009; *Menesguen et al.*, 2012; *Papenberg et al.*, 2010], currents [*Tang et al.*, 2013; *Tang and Zheng*, 2011; *Vsemirnova et al.*, 2012], internal waves [*Holbrook and Fer*, 2005; *Krahmann et al.*, 2008], and thermohaline staircases [*Biescas et al.*, 2010; *Fer et al.*, 2010].

While subsurface eddies (mostly Meddies) have been frequently studied using the seismic method [e.g., *Biescas et al.*, 2008; *Menesguen et al.*, 2012; *Pinheiro et al.*, 2010], only two surface anticyclonic eddies have been briefly reported. One is a joint oceanographic and seismic survey by *Mirshak et al.* [2010]. They presented a robust view but simple description of a surface eddy in the Gulf Stream region [*Mirshak et al.*, 2010]. The other targeted a large warm core ring eddy generated by the Kuroshio Extension off northeast Japan [*Yamashita et al.*, 2011]. Here we report a surface eddy (Yakutat eddy) at the head of the GoA, captured by two seismic lines of a marine 2-D seismic reflection cruise undertaken in autumn 2008. By merging our seismic observations with in situ hydrographic and satellite data (sea level anomaly and chlorophyll concentration), we present some of the eddy's properties, such as finescale structure, classification, scale, trajectory, translation speed, and geostrophic speed.

2. Data and Methods

In 2008, a 2-D marine seismic reflection experiment was conducted during the St. Elias Erosion/Tectonics Project (STEEP) aboard the R/V *Marcus G. Langseth* [*Christeson et al.*, 2010; *Gulick et al.*, 2013; *Worthington et al.*, 2010]. The seismic source was a tuned array of 36 BOLT guns (total volume of 6600 cu in, or 108 L) that were triggered every 50 m. Data were collected using a 636-channel streamer with 12.5 m channel spacing towed at 9 m. In the present study, 120 near-source traces and the first 4 s of the data were sampled for imaging. Two seismic transects STEEP13 (Line1, from 13:21, 17 September to 2:53, 18

September) and STEEP07 (Line2, from 6:53 to 19:53, 18 September) were reprocessed using the prestack depth migration method [*Liu and Bleistein*, 1995; *Tang and Zheng*, 2011]. A constant velocity model of 1480 m s^{-1} was used during the prestack depth migration simplified from the climatological mean velocities derived from the World Ocean Database 2009 (WOD09, www.nodc.noaa.gov).

Considering no available in situ hydrographic profile, we used satellite data to support the seismic observations. Multimission, merged, mapped sea level anomaly (SLA) data and the resultant by-products of geostrophic currents were collected from www.aviso.oceanobs.com, as well as the along-track altimeter data. Both SLA data and geostrophic velocity fields were used to detect the sea surface eddy on 17 September 2008 by three different algorithms: geometric-based stream function [*Nencioli et al*., 2010], physical-based Okubo-Weiss parameter [*Henson and Thomas*, 2008; *Isern-Fontanet et al*., 2003], and sea surface height [*Chelton et al*., 2011]. Among them, the Okubo-Weiss method is based on the parameter $W=s_s^2+s_n^2-\omega^2$, where s_s, s_n, and ω are, respectively, the shear deformation, the strain deformation, and the vorticity. Here, W quantifies the relative importance of deformation with respective to rotation. Ocean eddies are generally characterized by negative values of W because of inherent rotation dominated velocity fields. The high-resolution (~6 km) along-track altimeter data were also used to constrain the geometry of the observed eddy. The 7 day, 1/4° spatial resolution geostrophic velocity fields in 2008 were collected to track this eddy manually using the stream functions [*Nencioli et al*., 2010]. The Medium Resolution Imaging Spectrometer (MERIS, from http://oceancolor.gsfc.nasa.gov) 9 km monthly merged chlorophyll-a product of September 2008 was used to aid determination of eddy translation and coastal to pelagic water exchange.

In addition, we can estimate the section-normal geostrophic flow from the seismic transects. The long scale deformed isopycnals are related to geostrophic velocity field according to the thermal wind theory [*McWilliams*, 2006]. The geostrophic flow results from the balance of the Coriolis and horizontal pressure gradient forces, described by the Rossby number $Ro=\frac{U}{fL}$, where U and L are the characteristic velocity and length scale, f is the Coriolis parameter. If $Ro << 1$, the system is in geostrophic balance. For a two-dimensional section like the seismic line, vertical shear of the geostrophic flow normal to the transect could be estimated using the Margules formula, which is the discrete form of the thermal wind theory [*Margules*, 1906; *Sheen et al*., 2011]. Therefore, for a known slope γ of an isopycnal, the geostrophic vertical shear Δu across the isopycnal surface is estimated using: $\Delta u = g/f(\Delta\rho/\rho)\tan\gamma$, where the g is gravitational acceleration, $\Delta\rho$ is the change of the density across the isopycnal surface, and ρ is the mean density of two layers. Except for the geostrophic balance criterion, another important assumption is that the seismic horizons approximate isopycnal surfaces. This assumption has been proved to be applicable by *Krahmann et al*. [2009] so long as the periods of seismic data acquisition less than 4 h, i.e., seismic horizons are less than 36 km for the vessel speed at ~2.5 m s^{-1} (5 knot).

To reach the above-mentioned requirements in the GoA, the minimum length scale was estimated as follows: $f \sim 1.25 \times 10^{-4}$ s^{-1}, U~0.1 m s^{-1}, $Ro < 0.1$ for $L > 8$ km. Thus the seismic transects were discretized by a series of moving windows, whose sizes were 10 km (wide) × 100 m (deep) and moving steps were half-width horizontally and half-depth vertically. Seismic reflections were picked using the autotracking scheme and then smoothed. Horizons shorter than 3 km ($Ro \sim 0.3$) were discarded to reduce the disturbances from ageostrophic processes, such as internal waves. From the historical hydrographic data of WOD09, a mean density profile of autumn (August to October) near the study region (146°W ~ 142°W; 58.5°N ~ 59.5°N) was estimated, smoothed, and then resampled every 50 m. It was used to construct the one-dimensional density model. Once the geostrophic shear Δu across the windows were calculated, the absolute values of geostrophic flow were determined by vertically integrating from a level of known motion [*Sheen et al*., 2011]. Here, the reference depth was set to 1000 m where the geostrophic flow was around zero [*Thomson and Krassovski*, 2010]. In addition, we make use of the in situ sea surface temperature (SST) and salinity (SSS) data of Line2 (data are not available for Line1) from a shipboard Seabird SBE23 Thermosalinograph (TSG) to help to depict the eddy characteristics.

3. Results and Interpretations

During 17 and 18 September 2008, both seismic transects of Line1 and Line2 captured pronounced mesoscale anomalies from a nearly bowl-like structure, most likely a Yakutat eddy, which was further verified by tracking the anomalies on weekly SLA data. Eddy shape and scale were estimated by combining the along-track altimeter and seismic data, and then compared with the results from three conventional algorithms of eddy detection. Finally, the eddy-induced velocities were estimated based on the assumption of geostrophic balance.

3.1. Seismic Transects

Figures 2 and 3 show the water column finescale structures of Line1 and Line2 from 50 to 900 m depth. The most pronounced features of the sections are the bowl-like structure (A1) and an up-down asymmetric lens-like structure (A2). The anomaly A1 sits in the horizontal range from 15 to 70 km and vertical depth range from the surface to 700 m. A2 ranges from 15 to 55 km laterally and extends from surface down to 550 m vertically, much smaller than A1. The perfect left-right symmetry of their shapes look fine, indicating well-developed mesoscale structures. They are suggestive of anticyclonic surface eddies based on comparisons with either the schematic model [e.g., *Faghmous*, 2012] or the similar seismic observations [*Mirshak et al*., 2010; *Yamashita et al*., 2011]. Considering that (1) the spatial and temporal closeness with only ~15 km apart and ~12 h lag between the location/time the ship crossed the centers of A1 and A2 and (2) the nearly static (~3 km d^{-1}) translation of the eddy at this time scale, the two transects are therefore likely crossing the same eddy. Meanwhile, from the scales of A1 and A2, we can infer that the Line2 is farther from the eddy center and samples the eddy margin. This can be seen from the SLA or its derived maps in Figures 4 and 5.

Unlike most of the previously mapped subsurface eddies with single edge around the core [*Biescas et al*., 2008; *Pinheiro et al*., 2010], this surface eddy core (A1) is surrounded by two strong bands of reflectors, separated by an acoustically transparent zone ~50−100 m thick. The inner fringe is thicker than the outer one. Their thicknesses decrease monotonously from >100 m to a few tens of meters with increasing depth. The outer fringe tends to be disturbed in that its south (left) flank at around 200−400 m depth and at its base are strongly disrupted, blurred, or absent.

Similar to some of the Meddy cores, this surface eddy core (ranging from ~25 to 60 km at 250 m depth) is characterized by moderate to weak reflections centered around 250 m depth. Reflections in and out of the moderate reflection zone are weak to transparent, showing typical layered fine structures around the center. It is a lens-shaped core surrounded by the bowl-like edge. This shape is comparable to a previous hydrographic observation of a Yakutat eddy, whose upper edge is domed [*Ladd et al*., 2005].

Overall, this surface eddy is an onion-like structure with alternative reflective and blanking zones. Previous studies by *Song et al*. [2011] and *Menesguen et al*. [2012] have reported similar features of the subsurface Meddies. They suggested that the winding spiral arms might be responsible for those features. Considering the high degree of symmetry of the fringe in our study, it is unlikely that spiral arms can be responsible. However, it is certain that the alternating weak/strong reflective zones show water masses and boundaries of different thermal/salinity properties with different degrees of mixing, while the variations in slope of the horizons suggest differential rotation with different geostrophic velocities.

The fine structure of A2 is much simpler than A1. The structures are similar in that both anomalies show an intensive mixing zone with strongly disrupted/blurred reflections at the SW flank. The structures are different in that there are no distinct fringes wrapping around the eddy base in A2. Instead, there are distinct

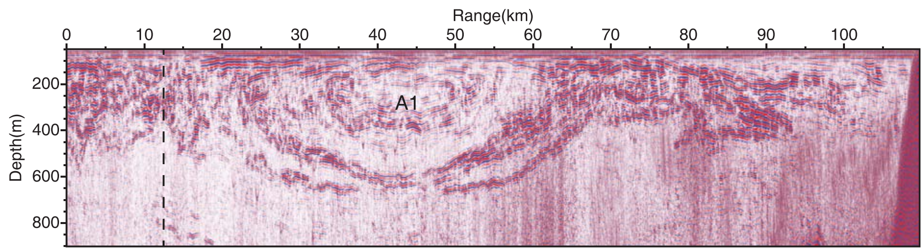

Figure 2. Depth migrated seismic image of Line1 (STEEP13) conducted from 13:21, 17 September to 2:53, 18 September 2008. A1 marks the bowl-like structure. The vertical dashed line is the intersection of Line2 shown in Figure 1.

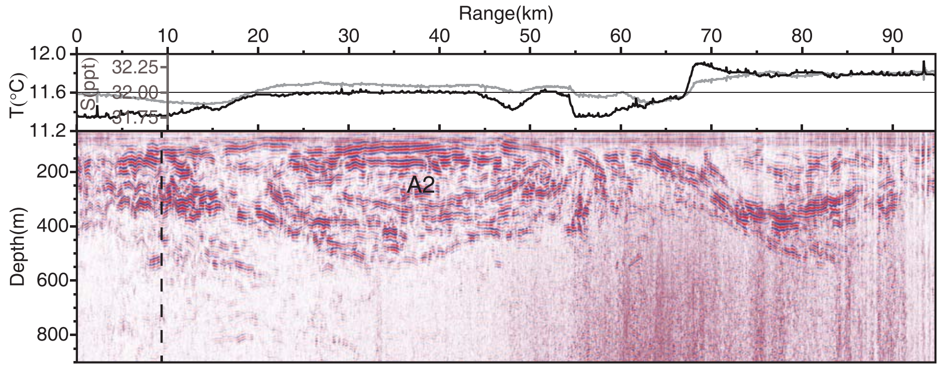

Figure 3. Depth migrated seismic image of Line2 (STEEP07) conducted from 6:53 to 19:53, 18 September 2008. A2 marks the lens-like structure. The vertical dashed line is the intersection of Line 1 shown in Figure 1. The top plot shows the in situ sea surface temperature (black) and salinity (gray).

patches of reflections winding around the NE eddy flank. We interpret that these observations show a typical spiral arm structure similar to the previous observations [*Menesguen et al.*, 2012; *Song et al.*, 2011]. The in situ observation of water properties also points to the spiral arm structure as described below. In the surrounding regions of A1 and A2, reflections are typically shallower extending to about 400−500 m depth. At the initial 15 km of the sections, especially near the southern edge of the eddy, the reflections are strongly undulating and disrupted with pervasive intermittency. This feature is typically suggestive of the enhanced diapycnal mixing [*Sheen et al.*, 2011]. From ∼75 km (Line1) and ∼65 km (Line2) to the end of the sections, two sets of strong northward dipping reflections show a similar frontal feature offshore the shelf-break, i.e., a shelf-break front with northwestward geostrophic flow, similar to the hydrographic observations by *Okkonen et al*. [2003] and *Ladd et al*. [2005]. Numerical modeling has shown that the shelf-break current in the GoA is the Alaska Current [*Hermann et al*., 2002]. Reflections below our observed eddy and in proximity are characterized by acoustic blanking or contaminated by vertically striped noise of seafloor multiples from previous shots.

The top plot of Figure 3 shows the in situ SST and SSS along Line2 from a shipboard TSG. High correlation between the varying SST and SSS reveals distinct water properties along the line, showing strong lateral variations of the mixed layer in the GoA. Further, both variations of SST and SSS correspond extremely well with the seismic anomalies. Flat cap-like curves of the SST/SSS outlined the eddy, showing relatively warmer/saltier of the eddy water than its surroundings. A small colder/fresher anomaly centered near 48 km is trapped by the warmer/saltier water on both sides. Such a phenomenon must be caused by the rotating eddy: a looping spiral arm shed from the warm/salty eddy entrained the cold/fresh water around it, further supporting the interpretation of the seismic data. A colder/fresher water zone with 10−20 km width is thought to be wrapping around the eddy, which might be undetectable using conventional site-based observations. The abrupt increase in both SST and SSS at 68 km pinpoints the outcrop of the shelf-break front (the Alaska Current) imaged by the seismic data.

3.2. Eddy Formation and Translation

According to the previous studies, there are two possible types of eddies, Yakutat eddies and Sitka eddies, could appear at the head of the GoA [*Henson and Thomas*, 2008; *Ladd et al*., 2005; *Rovegno et al*., 2009]. Here we tried to determine the eddy's formation region using the satellite altimetry. A geometry-based eddy detection algorithm [*Nencioli et al*., 2010] was applied to detect and track the eddy from the integrated stream functions of the geostrophic velocity fields.

Figure 4 shows the manually tracked result of the eddy in 2008 superimposed on the basemaps of both stream function and geostrophic velocity field on 17 September 2008. The pathway of the eddy seems complex in that two sections (dashed lines) close to the shelf-break are less robust than other sections (solid lines). The less robust sections may be caused by: (1) less well-determined geoid in the coastal areas, (2) unreliable near shore SLA data, (3) weak SLA embedded in a larger-scale background (≤ +5 cm, Figures 4 and 5c), and (4) interference or mergence with coastal anomalies. However, we still believed that these paths are acceptable for the following considerations: (a) successive positive anomalies, (b) spatial and

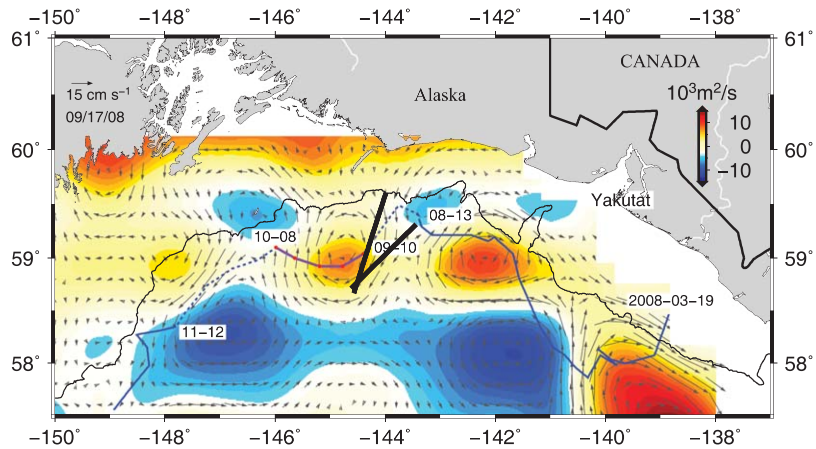

Figure 4. Map of stream-function field and the geostrophic velocities of the study region derived from sea level anomaly on 17 September 2008 distributed by Aviso (www.aviso.oceanobs.com/duacs). The unit of the stream function is 10^3 m^2 s^{-1} and its contour interval is one unit. Two black lines are the seismic transects. The polygonal line is the (possible) trajectory of the eddy tracked weekly using the stream-function method in the year 2008. The purple part is the convinced trajectory of the imaged eddy and the blue part is its possible trajectory. The solid parts of the trajectory are robust and the dashed parts are less robust.

temporal continuities, and (c) reasonable translation speeds (ca. 3–4 km d^{-1}). Therefore, we conclude that the eddy was formed on the continental shelf south of Yakutat, headed SW off the shelf into the basin, turned NW and then propagated around the GoA staying close to the shelf-break, and finally embedded in the Alaskan Stream. It was a long-lived eddy formed in March 2008 and was still alive at the end of that year after more than 9 month and 900 km traveled. Otherwise, if the less robust sections were rejected, the lifetime of the eddy was only around 1 month since 10 September 2008 with mean propagation speed of 3.5 km d^{-1} (purple line with red dots) formed right at the head of the GoA. Nevertheless, whatever the situation was, this eddy could be categorized as a Yakutat eddy in view of the possible formation sites being near the broad shelf region of Yakutat.

3.3. Eddy Shape and Scale

Since the seismic observations can outline the eddy edge precisely, we incorporated the high-resolution along-track altimeter data to best fit the eddy edge. Meanwhile, we tried to examine the reliability and rationality of the conventional algorithms based on the filtered altimeter data by AVISO. Because there is no universal definition of eddy edges [*Nencioli et al*., 2010], different algorithms always result in significant variation in eddy shapes and scales. There are numerous schemes that could be used to detect the eddy [e.g., *Chaigneau et al*., 2008; *Chelton et al*., 2011; *Nencioli et al*., 2010]. Here we applied three representative schemes to assess a range of results: (a) geometric-based stream-function method [*Nencioli et al*., 2010], (b) physical-based Okubo-Weiss parameter method [*Henson and Thomas*, 2008; *Isern-Fontanet et al*., 2003], and (c) sea surface height method [*Chelton et al*., 2011]. Once an eddy edge is delimited, the eddy area A is also determined. Then the equivalent diameter $\bar{D}$, corresponding to a circular eddy having the same area A, can be calculated using $\bar{D}=2\sqrt{\frac{A}{\pi}}$.

The red outlines in Figure 5 show the results from different eddy detection schemes. Blue highlighted portions of the two seismic transects that include the mapped spatial extents of the eddy. All three methods detected the eddy successfully with nearly identical centers. However, the edges of the detected eddy in the three schemes do not equally satisfy the seismic observations, especially for the Line2. Line1 crosses different portions of the eddy edges, while the edges are completely missed on Line2 as the section is almost tangential to the edges. The along-track altimeter data and seismic data provide an improved oval-shaped eddy (Figure 5d) satisfying both types of high-resolution observations. The discrepancies between the individual conventional schemes and seismic observation are invisible on the SW side but significant on the NE side, indicating less reliability of the filtered SLA data close to the shelf.

The equivalent diameters $\bar{D}$ of the closed edges estimated based on the equal area criterion are ~50 km for the stream-function method and ~65 km for the Okubo-Weiss parameter method, the sea surface height method, and the best fit method (Figure 5). Therefore, we consider that the edge constraints of the stream-

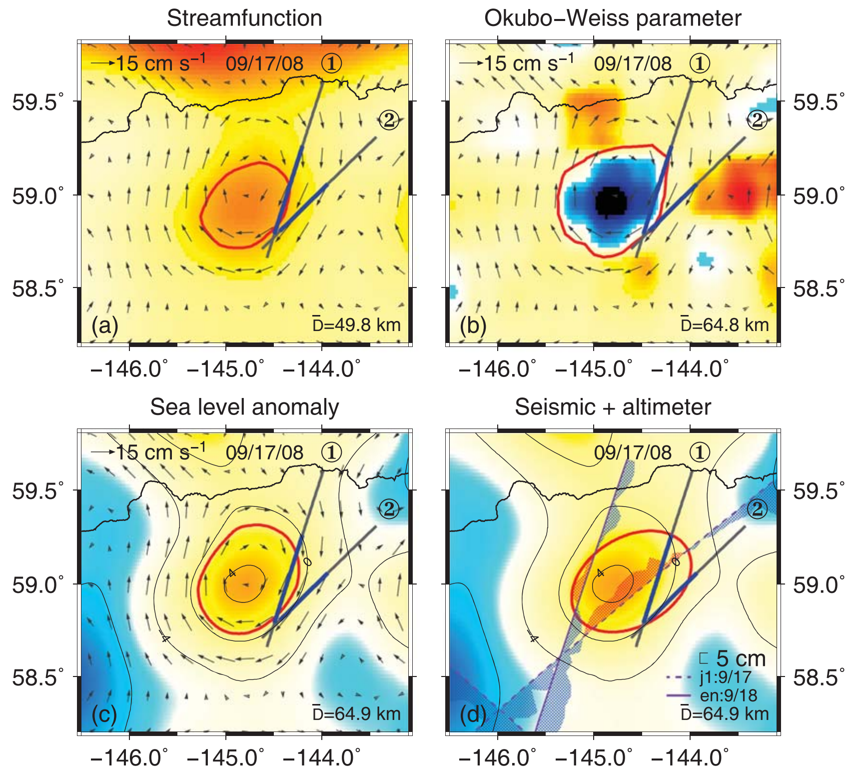

Figure 5. Comparisons of different eddy detection methods. (a) Geometric-based stream-function method. (b) Physical-based Okubo-Weiss parameter method. (c) Sea surface height method. (d) The improved eddy edge fitting using both along-track altimeter data and seismic data. The blue portions of the seismic lines are the locations of the imaged eddy. The closed red lines are the edges of the detected eddy. Their corresponding equivalent diameters $\bar{D}$ (equal area based) are shown at the bottom right of the figures. Wiggles in Figure 5d shaded with red (positive) and blue (negative) are the along-track altimeter data extracted from satellite Jason-1 (j1, purple dashed) and Envisat (en, purple), respectively.

function method should be improved, because this method underestimated the eddy size relative to the other methods, similar to the tests reported by *Nencioli et al*. [2010]. The eddy sizes derived from the Okubo-Weiss parameter method and the sea surface height method are very similar, and nearly identical to the best fit method. Such mutual consistency shows that these methods could be viewed as reliable for the eddy size estimation. Therefore, the estimated diameter of this Yakutat eddy is around 65 km. It is a rather small eddy compared with previous observations with a typical range of 80−200 km in diameter [e.g., *Henson and Thomas*, 2008].

3.4. Eddy Velocity Field

Using the approximate isopycnals (Figures 6a and 7a) tracked from the seismic transects Line1 and Line2 (Figures 2 and 3), we estimate the geostrophic flow field normal to the seismic transects (Figures 6b and 7b). Similar to the result of a low pressure system (cyclonic eddy) by *Sheen et al*. [2011], our result reveals the cross-section velocities of a high pressure system (a Yakutat anticyclonic eddy) and a strong shelf-break current, probably the Alaska Current [*Hermann et al*., 2002].

Geostrophic velocity fields of the eddy show anticyclonic features with flow reversal across narrow zones at $\sim$43 km in Line1 and $\sim$38 km in Line2 (Figures 2 and 3). The overall symmetry of the field shape in Line1 is better than in Line2. However, a prominent feature is the asymmetric strength of the eddy velocity field between the near-basin side ($\sim$10 cm s^{-1}) and near-shelf side ($\sim$20 cm s^{-1}) in Line1. The estimated geostrophic transports into and out of the transect are around 1.06 and 1.90 Sv (1Sv $\equiv 10^6$ m^3 s^{-1}), respectively. In Line2, the velocity values are typically $\pm$0.05 cm s^{-1} with transports into and out of the transect around 0.56 and 0.29 Sv. There are two primary factors might be responsible for the transport differences: (1) unequal normal components of the velocity field and/or (2) entrainment or detrainment of the eddy [*Stern*, 1987], such as intrusions, spiral arms and their accompanying ageostrophic effects. There is a strong NW

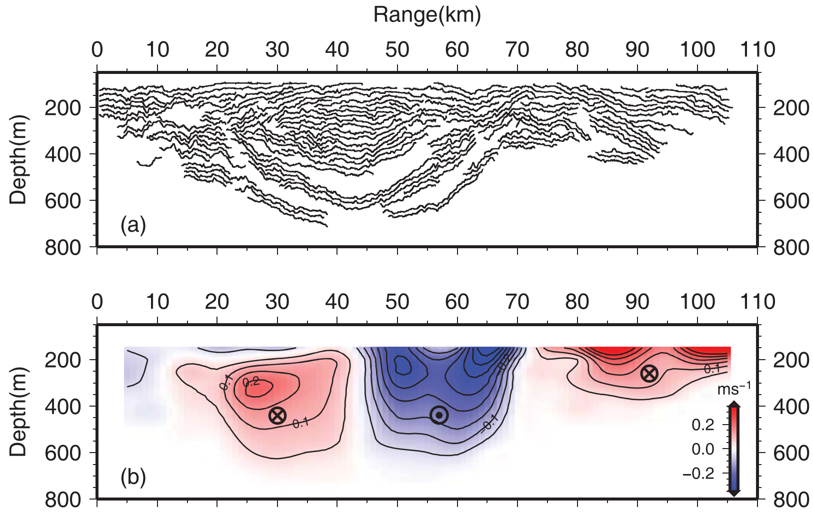

Figure 6. (a) Tracked horizons from seismic transect Line1. (b) Velocity field perpendicular to Line1. Current coming out of the paper is shaded with blue (circle with a dot). Current flowing into the paper is shaded with red (circle with a cross).

current (Alaska Current) that passes by the eddy along the shelf-break with velocity up to 40 cm s^{-1} at 150 m depth in the core region. Its estimated transport is around 0.79 and 1.03 Sv for Line1 and Line2, respectively. Our results of the estimated velocity field cannot be well matched with the surface geostrophic flow (e.g., Figure 4), especially for the Alaska Current on the near-shelf side. Missing evidence for the Alaska Current in the surface geostrophic field further indicates that the near shore altimeter data are negatively affecting the eddy detection results.

Geostrophic flow estimation from the seismic data is influenced by several aspects, such as the ageostrophic components, simplified density model, isopycnal approximation, and initial integrating velocities. The ageostrophic components disturb the slopes of the horizons and finally affect the geostrophic shear. Typical error in a window (10 km $\times$ 100 m) below and above 250 m depth is less than 2 and 5 cm s^{-1}, respectively. Simplification of the 1-D density model from the historical data could introduce errors by ignoring the lateral density variations of the eddies, whose isopycnals are typically depressed more than 150 m [*Ladd et al.*, 2005]. Further, approximation between the seismic reflectors (mostly dependent on temperature) and the isopycnal surfaces will bring errors because reflectors do not always follow isopycnals, especially near subsurface eddies. Seismic reflectors are apt to overestimate the isopycnal slopes significantly [*Biescas et al.*, 2013]. However, the overestimation may be well reduced for the surface eddies as

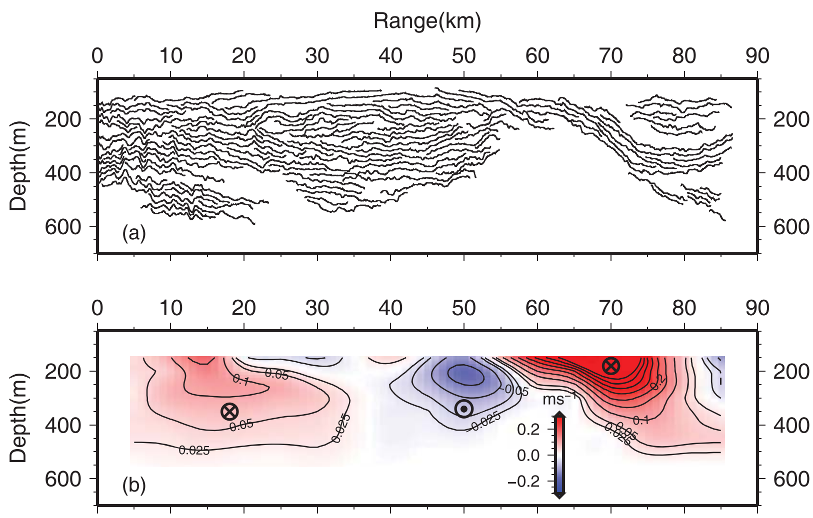

Figure 7. Same as Figure 6, but for the seismic transect Line2.

observations only show minor discrepancies between the isothermals and the isopycnals [*Ladd*, 2007; *Ladd et al*., 2005]. Errors from the initial velocity model are obvious in view of the conflicts between the surface geostrophic flow and the integrated flow. However, our results are as expected, based on the pattern and strength of our integrated flow for both the eddy and current. In this study, without the in situ current measurement, it would be unreasonable to integrate the geostrophic shear from top to bottom because of the harm of the cumulative errors resulting from the shallow pycnocline, where the density variations are extremely large in a given window. However, both previous hydrographic observations [*Thomson and Krassovski*, 2010] and our estimation show a weak geostrophic field of 1−2 cm s^{-1} at 800 m depth. Therefore, it is more reasonable to be the reference depth for integrating at the 1000 m depth than the ocean surface.

The effect of the centrifugal force should be considered due to the curved flow trajectory. Assuming a circular eddy, we estimated the azimuthal velocity corrections by introducing the centripetal acceleration v^2/r under the cyclo-geostrophic regime: $fv + v^2/r - fv_g = 0$. Thus the equation can be solved analytically for v with result: $v = \frac{2v_g}{1 \pm \sqrt{1+4v_g/(fr)}}$. We found that most of the geostrophic velocities in Line1 require corrections less than +15% approximately.

4. Discussion

Yakutat eddies can carry shelf water into the GoA basin. The high-resolution in situ TSG data help us to understand such a process from the properties of the eddy and its surrounding waters. Figure 8 presents the SST/SSS along the vessel track on 18 September 2008. The most interesting feature is that the warm salty eddy was surrounded by a cold and fresh water zone with 10−20 km width, probably a long filament which might be missed using the site-based observation. Spatially, this water zone is corresponding well with the inferred diapycnal mixing zone on the seismic transects. However, it would be misleading if we believe that this cold water zone is caused only from the diapycnal upwelling and downwelling. Because diapycnal mixing may be caused by a saltier surface water zone (salt conservation) conflicting with the freshest water zone observed along the track. Similarly, the lateral interleaving between the

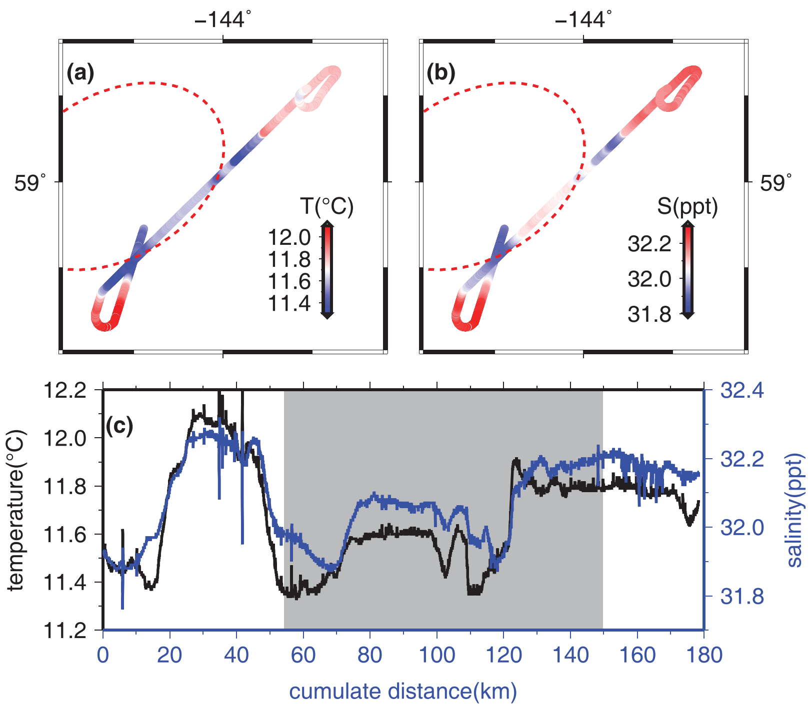

Figure 8. (a) In situ temperature along the vessel track on 18 September 2008. Red circle is the eddy edge shown in Figure 5d. (b) Same as Figure 8a but for the salinity. (c) The temperature (black) and salinity (blue) along the cumulative track from approximately SW to NE. Gray part is the Line2 same as in Figure 3.

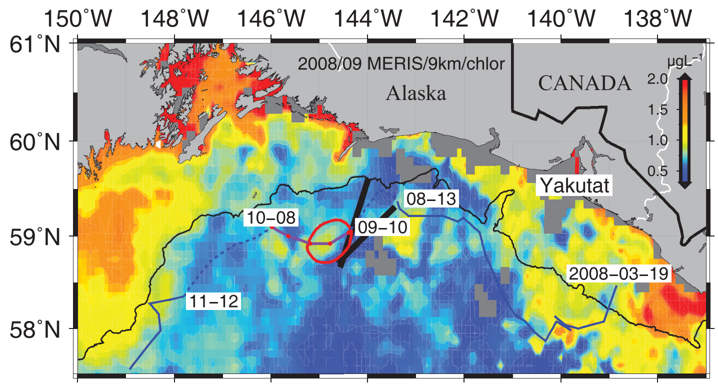

Figure 9. Average Surface chlorophyll-a concentrations (μg L^{-1}) in September 2008 from MERIS (http://oceancolor.gsfc.nasa.gov). Red line is the eddy edge shown in Figure 5a. Other annotations are same as in Figure 4.

warm salty eddy and the warm salty surrounding waters cannot form cold and fresh water either. Therefore, we suggest that the cold and fresh water zone was entrained from somewhere else, most likely the northern shelf-break, and then wrapped around the eddy when the eddy was impinging or sliding over the shelf-break. Such a process could be verified from the Argo drifters' behavior: pulled seaward of the shelf-break by the eddy and then looped around the outside edge of the eddy [*Ladd et al.*, 2007]. Further, it might influence the species distributions, e.g., jellyfish, as described by *Ladd et al.* [2005] along the physical gradients [*Graham et al.*, 2001].

Anticyclonic eddies in the northern GoA have been implicated in high chlorophyll concentrations observed from ocean color satellites [*Ladd*, 2007]. Eddies near the continental margin transport nutrient-rich coastal waters into pelagic regions by entraining coastal water and then advecting them into the basin interior to increase phytoplankton populations there [*Crawford et al.*, 2007]. The map of surface chlorophyll concentration in September 2008 by MERIS shows a spread area with high chlorophyll anomaly close to the eddy (Figure 9). The spatial distribution of the anomaly corresponds well with the trajectory of the observed Yakutat eddy during September 2008. This correspondence is another indication of the water transport process from the nutrient-rich coastal region into the low chlorophyll basin interior through the eddy translation.

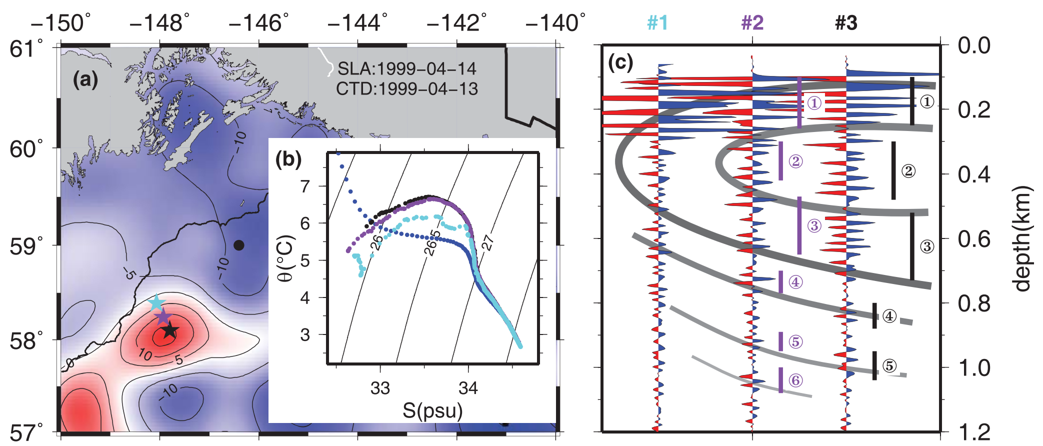

Figure 10. (a) Map of the SLA on 14 April 1999. CTD casts (color stars, 13 April 1999) sampled the NW flank of an eddy used for comparison. It was a young anticyclonic eddy formed in March 1999 near the head of GoA (black dot). (b) $\theta - S$ diagram for the CTD casts (colored correspondingly) and reference curve (blue) of the climatological temperature-salinity profile. (c) Synthetic seismograms derived from the CTD casts using a Ricker wavelet with central frequency of 50 Hz. Details of the "reflection" zonation (numbered lines) are discussed in the text. Gray lines outline a possible eddy structure with multiple striae.

Seismic image of the Yakutat eddy (Figure 2) shows a detailed feature of double fringes separated by homogeneous waters. It presents an interesting eddy phenomenon with thin striae around the base. To examine whether this is a universal feature of an eddy in the GoA, we searched the archives of the WOD09 for data just sampling the edge of any eddies to synthesize the seismograms. Fortunately, we found three CTD profiles sampling an earlier eddy from NW edge to the center acquired on 13 April 1999 (Figure 10a). This eddy first appeared near the head of the GoA (black dot in Figure 10a), very close to the formation region of the eddies reported by *Crawford et al*. [2000] and *Ladd et al*. [2007]. The CTD profiles show typical warm salty water relative to basin water of the same density (Figure 10b). Their synthesized seismograms from the temperature/salinity data are shown in Figure 10c. We can clearly see the varying trends of the "reflections" from the eddy edge to the center. Roughly, the "reflections" could be divided into several segments of the alternating weak/strong "reflective" zones as noted nearby the seismograms. By comparing with the imaged Yakutat eddy, we can infer that the segments 1 and 3 are the upper and lower edge of the eddy, and segment 2 is the eddy center. Segments 4, 5, and 6 should be the outer thin striae similar to our imaged eddy. Without loss of generality, vertical structures derived from the CTD data may indicate that the wrapping of striae around an eddy base is a common feature, at least for eddies in the GoA. One possible explanation for the feature is the strongly depressed isotherms/isopycnals (distinct water boundaries; temperature profiles with only negative gradients, not shown here), rather than the water boundaries of a cold tongue wrapping around the warm eddy as reported by *Mirshak et al*. [2010].

In addition, the key point of the geostrophic velocity estimation from the seismic image is highlighted in practice, i.e., seismic reflectors (mostly dependent on temperature) do not always follow isopycnals. Before applying the geostrophic estimation, it should be checked that whether isothermals and isopycnals are in accordance with each other. For example, surface mesoscale eddies in the GoA region always show the minor discrepancies between the isothermals and isopycnals. Thus seismic reflector slopes could be the suitable substitutes for isopycnal slopes. Nevertheless, errors from the ageostrophic components, density model, and initial integrating velocities make the estimated geostrophic velocities unmatchable with the surface geostrophic flow, whose error is also remarkable especially near the coastal regions. In contrast, differences between the isothermals and isopycnals of the subsurface eddies are much more significant according to the report by *Biescas et al*. [2013]. In such a case, it would be inappropriate to apply the geostrophic velocity estimation using the seismic reflector slopes. In all, careful analyses of the applicability and errors of this method are necessary. After the geostrophic velocities are seismically derived, if possible, the velocity corrections induced by the centrifugal forces should be estimated under the cyclo-geostrophic regime.

5. Conclusions

In this work, detailed structures of a surface anticyclonic eddy and a shelf-break current have been unveiled by reprocessing two 2008 seismic transects at the head of the GoA. The eddy is a typical bowl-like structure with around 55 km width and 700 m depth. It has two fringes around the eddy base. The in situ SST/SSS data help us to confirm a spiral arm shed from the warm eddy and the entrained cold water from somewhere else. Nearby the eddy and offshore the shelf-break, there is a strong frontal feature, most probably related to the Alaska Current.

Combining with the altimeter data, we tracked the eddy to determine its generation site, and categorized it as a Yakutat eddy. Then we achieved the equivalent eddy diameter of 65 km using the high-resolution along-track altimeter and the seismic constraints. Meanwhile, three representative conventional algorithms of eddy detection were presented for comparison. We found that the Okubo-Weiss parameter and sea surface height method are nearly identical to our result, although their shapes differ especially near the shelf-break. However, the eddy size was underestimated by the stream-function method. The geostrophic velocities of the Yakutat eddy and the Alaska Current were also estimated from the deformed "isopycnals" under the assumption of geostrophic balance.

Further, the in situ SST/SSS data help us to reveal the properties and dynamic processes of the water masses. For example, we found that a narrow zone of the cold and fresh water was entrained from the northern shelf-break and wrapped around the eddy. The chlorophyll concentration also shows the water transport process from the nutrient-rich coastal region into the low chlorophyll basin interior through the eddy translation. Finally, we searched the historical hydrographic profiles sampling an earlier eddy to synthesize the seismograms, showing that the thin striae around the eddy base might be a common feature in the GoA.

Acknowledgments
We thank the captain, crew, and science party of R/V *Marcus G. Langseth* cruise MGL0814 for acquiring the STEEP seismic data, courtesy of the Marine Geoscience Data System (MGDS; www.marine-geo.org). The altimeter products were produced by Ssalto/Duacs and distributed by the AVISO, with support from the CNES (www.aviso.oceanobs.com/duacs). The MERIS chlorophyll products and the historical CTD profiles are available from http://oceandata.sci.gsfc.nasa.gov and www.nodc.noaa.gov, respectively. This research was supported financially by the NSFC (grants 41176026 and 41376023) and the NSF (grants EAR-0408584 and EAR-1009986). This is UTIG contribution #2708.

References

Biescas, B., V. Sallares, J. L. Pelegri, F. Machin, R. Carbonell, G. Buffett, J. J. Danobeitia, and A. Calahorrano (2008), Imaging meddy finestructure using multichannel seismic reflection data, *Geophys. Res. Lett.*, *35*, L11609, doi:10.1029/2008GL033971.
Biescas, B., L. Armi, V. Sallares, and E. Gracia (2010), Seismic imaging of staircase layers below the Mediterranean Undercurrent, *Deep Sea Res., Part I*, *57*(10), 1345–1353, doi:10.1016/j.dsr.2010.07.001.
Biescas, B., B. Ruddick, and V. Sallares (2013), Inversion of density in the ocean from seismic reflection data, *J. Acoust. Soc. Am.*, *133*(5), 3312, doi:10.1121/1.4805509.
Buffett, G. G., B. Biescas, J. L. Pelegri, F. Machin, V. Sallares, R. Carbonell, D. Klaeschen, and R. Hobbs (2009), Seismic reflection along the path of the Mediterranean Undercurrent, *Cont. Shelf Res.*, *29*(15), 1848–1860, doi:10.1016/j.csr.2009.05.017.
Chaigneau, A., A. Gizolme, and C. Grados (2008), Mesoscale eddies off Peru in altimeter records: Identification algorithms and eddy spatio-temporal patterns, *Prog. Oceanogr.*, *79*(2–4), 106–119, doi:10.1016/j.pocean.2008.10.013.
Chelton, D. B., M. G. Schlax, and R. M. Samelson (2011), Global observations of nonlinear mesoscale eddies, *Prog. Oceanogr.*, *91*(2), 167–216, doi:10.1016/j.pocean.2011.01.002.
Christeson, G. L., S. P. S. Gulick, H. J. A. van Avendonk, L. L. Worthington, R. S. Reece, and T. L. Pavlis (2010), The Yakutat terrane: Dramatic change in crustal thickness across the Transition fault, Alaska, *Geology*, *38*(10), 895–898, doi:10.1130/G31170.1.
Crawford, W. R. (2002), Physical characteristics of Haida Eddies, *J. Oceanogr.*, *58*(5), 703–713, doi:10.1023/A:1022898424333.
Crawford, W. R., J. Y. Cherniawsky, and M. G. G. Foreman (2000), Multi-year meanders and eddies in the Alaskan Stream as observed by TOPEX/Poseidon altimeter, *Geophys. Res. Lett.*, *27*(7), 1025–1028, doi:10.1029/1999GL002399.
Crawford, W. R., P. J. Brickley, and A. C. Thomas (2007), Mesoscale eddies dominate surface phytoplankton in northern Gulf of Alaska, *Prog. Oceanogr.*, *75*(2), 287–303, doi:10.1016/j.pocean.2007.08.016.
Faghmous, J. H. (2012), Eddyscan: A physical consistent ocean eddy monitoring application, paper presented at 2012 Conference on Intelligent Data Understanding National Center for Atmospheric Research, Boulder, Colo.
Fer, I., P. Nandi, W. S. Holbrook, R. W. Schmitt, and P. Paramo (2010), Seismic imaging of a thermohaline staircase in the western tropical North Atlantic, *Ocean Sci.*, *6*(3), 621–631, doi:10.5194/os-6–621-2010.
Graham, W. M., F. Pages, and W. M. Hamner (2001), A physical context for gelatinous zooplankton aggregations: A review, *Hydrobiologia*, *451*(1–3), 199–212.
Gulick, S. P. S., R. S. Reece, G. L. Christeson, H. van Avendonk, L. L. Worthington, and T. L. Pavlis (2013), Seismic images of the Transition fault and the unstable Yakutat-Pacific-North American triple junction, *Geology*, *41*(5), 571–574, doi:10.1130/G33900.1.
Henson, S. A., and A. C. Thomas (2008), A census of oceanic anticyclonic eddies in the Gulf of Alaska, *Deep Sea Res., Part I*, *55*(2), 163–176, doi:10.1016/j.dsr.2007.11.005.
Hermann, A. J., D. B. Haidvogel, E. L. Dobbins, and P. J. Stabeno (2002), Coupling global and regional circulation models in the coastal Gulf of Alaska, *Prog. Oceanogr.*, *53*(2–4), 335–367, doi:10.1016/S0079–6611(02)00036-8.
Holbrook, W. S., and I. Fer (2005), Ocean internal wave spectra inferred from seismic reflection transects, *Geophys. Res. Lett.*, *32*, L15604, doi:10.1029/2005GL023733.
Holbrook, W. S., P. Paramo, S. Pearse, and R. W. Schmitt (2003), Thermohaline fine structure in an oceanographic front from seismic reflection profiling, *Science*, *301*(5634), 821–824.
Isern-Fontanet, J., E. Garcia-Ladona, and J. Font (2003), Identification of marine eddies from altimetric maps, *J. Atmos. Oceanic Technol.*, *20*(5), 772–778.
Krahmann, G., P. Brandt, D. Klaeschen, and T. Reston (2008), Mid-depth internal wave energy off the Iberian Peninsula estimated from seismic reflection data, *J. Geophys. Res.*, *113*, C12016, doi:10.1029/2007JC004678.
Krahmann, G., C. Papenberg, P. Brandt, and M. Vogt (2009), Evaluation of seismic reflector slopes with a Yoyo-CTD, *Geophys. Res. Lett.*, *36*, L00D02, doi:10.1029/2009GL038964.
Ladd, C. (2007), Interannual variability of the Gulf of Alaska eddy field, *Geophys. Res. Lett.*, *34*, L11605, doi:10.1029/2007GL029478.
Ladd, C., N. B. Kachel, C. W. Mordy, and P. J. Stabeno (2005), Observations from a Yakutat eddy in the northern Gulf of Alaska, *J. Geophys. Res.*, *110*, C03003, doi:10.1029/2004JC002710.
Ladd, C., C. W. Mordy, N. B. Kachel, and P. J. Stabeno (2007), Northern Gulf of Alaska eddies and associated anomalies, *Deep Sea Res., Part I*, *54*(4), 487–509, doi:10.1016/j.dsr.2007.01.006.
Ladd, C., W. R. Crawford, C. E. Harpold, W. K. Johnson, N. B. Kachel, P. J. Stabeno, and F. Whitney (2009), A synoptic survey of young mesoscale eddies in the Eastern Gulf of Alaska, *Deep Sea Res., Part II*, *56*(24), 2460–2473, doi:10.1016/j.dsr2.2009.02.007.
Liu, Z. Y., and N. Bleistein (1995), Migration velocity analysis - theory and an iterative algorithm, *Geophysics*, *60*(1), 142–153.
Margules, M. (1906), Uber Temperaturschichtung in stationarbewegter und ruhender Luft (on temperature stratification in steadily moving and calm air), *Meteorol. Z.*, *23*, 241–244.
McWilliams, J. C. (2006), *Fundamentals of Geophysical Fluid Dynamics*, vol. xvii, 249 p., Cambridge Univ. Press, N. Y.
Menesguen, C., B. L. Hua, X. Carton, F. Klingelhoefer, P. Schnurle, and C. Reichert (2012), Arms winding around a meddy seen in seismic reflection data close to the Morocco coastline, *Geophys. Res. Lett.*, *39*, L05604, doi:10.1029/2011GL050798.
Mirshak, R., M. R. Nedimovic, B. J. W. Greenan, B. R. Ruddick, and K. E. Louden (2010), Coincident reflection images of the Gulf Stream from seismic and hydrographic data, *Geophys. Res. Lett.*, *37*, L05602, doi:10.1029/2009GL042359.
Nencioli, F., C. M. Dong, T. Dickey, L. Washburn, and J. C. McWilliams (2010), A vector geometry-based eddy detection algorithm and its application to a high-resolution numerical model product and high-frequency radar surface velocities in the Southern California Bight, *J. Atmos. Oceanic Technol.*, *27*(3), 564–579, doi:10.1175/2009jtecho725.1.
Okkonen, S. R., G. A. Jacobs, E. J. Metzger, H. E. Hurlburt, and J. F. Shriver (2001), Mesoscale variability in the boundary currents of the Alaska Gyre, *Cont. Shelf Res.*, *21*(11–12), 1219–1236, doi:10.1016/S0278–4343(00)00085-6.
Okkonen, S. R., T. J. Weingartner, S. L. Danielson, D. L. Musgrave, and G. M. Schmidt (2003), Satellite and hydrographic observations of eddy-induced shelf-slope exchange in the northwestern Gulf of Alaska, *J. Geophys. Res.*, *108*(C2), 3033, doi:10.1029/2002JC001342.
Papenberg, C., D. Klaeschen, G. Krahmann, and R. W. Hobbs (2010), Ocean temperature and salinity inverted from combined hydrographic and seismic data, *Geophys. Res. Lett.*, *37*, L04601, doi:10.1029/2009GL042115.

Peterson, T. D., F. A. Whitney, and P. J. Harrison (2005), Macronutrient dynamics in an anticyclonic mesoscale eddy in the Gulf of Alaska, *Deep Sea Res., Part II*, *52*(7–8), 909–932, doi:10.1016/j.dsr2.2005.02.004.
Pinheiro, L. M., H. B. Song, B. Ruddick, J. Dubert, I. Ambar, K. Mustafa, and R. Bezerra (2010), Detailed 2-D imaging of the Mediterranean outflow and meddies off W Iberia from multichannel seismic data, *J. Mar. Syst.*, *79*(1–2), 89–100, doi:10.1016/j.jmarsys.2009.07.004.
Rovegno, P. S., C. A. Edwards, and K. W. Bruland (2009), Observations of a Kenai eddy and a Sitka eddy in the Northern Gulf of Alaska, *J. Geophys. Res.*, *114*, C11012, doi:10.1029/2009JC005451.
Ruddick, B., H. B. Song, C. Z. Dong, and L. Pinheiro (2009), Water column seismic images as maps of temperature gradient, *Oceanography*, *22*(1), 192–205.
Sheen, K. L., N. White, C. P. Caulfield, and R. W. Hobbs (2011), Estimating geostrophic shear from seismic images of oceanic structure, *J. Atmos. Oceanic Technol.*, *28*(9), 1149–1154, doi:10.1175/Jtech-D-10–05012.1.
Song, H. B., L. M. Pinheiro, B. Ruddick, and F. C. Teixeira (2011), Meddy, spiral arms, and mixing mechanisms viewed by seismic imaging in the Tagus Abyssal Plain (SW Iberia), *J. Mar. Res.*, *69*(4–6), 827–842.
Stabeno, P. J., N. A. Bond, A. J. Hermann, N. B. Kachel, C. W. Mordy, and J. E. Overland (2004), Meteorology and oceanography of the Northern Gulf of Alaska, *Cont. Shelf Res.*, *24*(7–8), 859–897, doi:10.1016/j.csr.2004.02.007.
Stern, M. E. (1987), Horizontal entrainment and detrainment in large-scale eddies, *J. Phys. Oceanogr.*, *17*(10), 1688–1695.
Tang, Q. S., and C. Zheng (2011), Thermohaline structures across the Luzon Strait from seismic reflection data, *Dyn. Atmos. Oceans*, *51*(3), 99–113, doi:10.1016/j.dynatmoce.2011.02.001.
Tang, Q. S., D. X. Wang, J. B. Li, P. Yan, and J. Li (2013), Image of a subsurface current core in the southern South China Sea, *Ocean Sci.*, *9*, 631–638, doi:10.5194/os-9–631-2013.
Thomson, R. E., and M. V. Krassovski (2010), Poleward reach of the California Undercurrent extension, *J. Geophys. Res.*, *115*, C09027, doi:10.1029/2010JC006280.
Vsemirnova, E. A., R. W. Hobbs, and P. Hosegood (2012), Mapping turbidity layers using seismic oceanography methods, *Ocean Sci.*, *8*(1), 11–18, doi:10.5194/Os-8–11-2012.
Worthington, L. L., S. P. S. Gulick, and T. L. Pavlis (2010), Coupled stratigraphic and structural evolution of a glaciated orogenic wedge, offshore St. Elias orogen, Alaska, *Tectonics*, *29*, TC6013, doi:10.1029/2010TC002723.
Yamashita, M., K. Yokota, Y. Fukao, S. Kodaira, S. Miura, and K. Katsumata (2011), Seismic reflection imaging of a warm core ring south of Hokkaido, *Explor. Geophys.*, *42*, 18–24, doi:10.1071/EG11004.

